Available online at www.sciencedirect.com

ScienceDirect

Procedia CIRP 108 (2022) 477–482

www.elsevier.com/locate/procedia

6th CIRP Conference on Surface Integrity

PIM-like EAM of steel-tool alloy via bio-based polymer

N. Charpentier [a]*, T. Barrière [a], F. Bernard [b], N. Boudeau [a], A. Gilbin [a], P. Vikner [c]

a. Univ. Bourgogne Franche-Comté, FEMTO-ST Institute, CNRS/UFC/ENSMM/UTBM, Department of Applied Mechanics, 24 chemin de l'Epitaphe, 25000 Besançon, France

b. Laboratoire Interdisciplinaire Carnot de Bourgogne - UMR 6303 CNRS/Université Bourgogne Franche-Comté, 9, Avenue Alain Savary BP 47870, Cedex, Dijon, 21078, France

c. . Aubert & Duval, Rue du Villa, 63770 Les Ancizes, France

* Corresponding author. Tel.: +33 (0)6 38 58 02 54; *E-mail address:* nicolas.charpentier@femto-st.fr

Abstract

This paper discusses an innovative additive manufacturing process, using a combination of polymer 3D printing by fused filament fabrication and powder metallurgy to create complex shaped, high density parts from powders without tooling. This process offers interesting prospects for reducing material waste and costs for prototyping or small series, as it does not require specific equipment. In this current work, the selected powder is a steel-tool alloy. The study covers the whole process, from the development of the feedstock material to its shaping including debinding and sintering steps, in order to manage all the steps to achieve a final component without defects and excellent mechanical and physical properties.

Keywords: Additive manufacturing; Powder Metallurgy; PIM-like EAM; Extrusion-based Additive Manufacturing; Polylactic Acid; Steel-tool alloy

1. Introduction

Extrusion-based Additive Manufacturing (EAM) [1] consists of controlling the extrusion of a viscous material through a nozzle. The part is built layer by layer with a nozzle animated of X-Y movements combined with a Z translation of the building plate.

The main advantages are that it allows to create complex geometries impossible to achieve with conventional processes and it needs no additional tools or dies. But it is limited for prototyping or for small production volumes. At the present time, this process is widely studied, essentially for conventional thermoplastic polymers like polylactic acid (PLA) or acrylonitrile butadiene styrene (ABS).

Like in Powder Injection Molding, a viscous material, loaded with solid powder, can be used as a vector for shaping material. Water-based slurry of metals or ceramics are generally used in robocasting [2], while polymer-based feedstock is used in 3D printing [3-5].

Powder Injection Molding (PIM) involves the use of a feedstock in an injection molding process followed by a debinding step and a sintering one [6]. The feedstock is obtained during the mixing stage where a thermoplastic polymer is combined with solid powders. During the debinding stage, the polymer binder is removed resulting in a porous material. During the sintering step, the porous material is densified. The common thermoplastic polymers used in injection molding are polypropylene, polyethylene or polyacetal [6]. In order to obtain homogeneous feedstocks with a high powder loading, some surfactants are used like acid stearic (SA) or paraffin wax [6]. The advantage of injection molding process is to obtain 3D parts with quite complex shape with a high-volume production. The debinding stage consists in eliminating the polymer by thermal degradation or chemical decomposition [6].

2212-8271
10.1016/j.procir.2022.04.077

Finally, the consolidation stage is realized by solid state diffusion with conventional [6] or innovative sintering processes [7]. The innovative sintering processes are performed by microwave assisted or spark plasma sintering. Royer et al. propose to employ some bio-sourced polymers as binder and more precisely a polylactic acid (PLA).

Moreover, contrary to other process, the material is not melted during the process, so difficult to weld materials such as high carbon tool steel can be shaped. PIM is a mature process with a wide range of appropriate materials such as stainless steel, titanium, superalloy and intermetallic alloys [7]. The final metallic components are characterized by a high density and a homogeneous microstructure. The mechanical properties are close to those of the solid material.

EAM and PIM processes can be combined to produce highly complex and low-cost full dense metallic or ceramic components [8]. This hybrid process has been recently applied to powder forming process with conventional metal powders such as 17-4 PH or 316L [9-10].

The present paper is devoted to the development of an innovative bio-sourced polymer binder formulation for the application of this hybrid process. The aim is to shape a tool-steel alloy powder. The debinding stage is realized by thermal degradation [12] and the densification is obtained by natural sintering [13]. In section 2, the description of the binder, powders and feedstock elaboration is described. In section 3, the combined EAM and PIM processes are developed and investigated. A special printing equipment is used where polymer granules, filled with tool-steel alloy powder, are used in place of a classical wire. In section 4, SEM analysis and physical properties, like the porosity and the surface roughness, are presented. In particular, their evolution, between the 3D printed step and the final sintered step, is from the 3D print to the final sintered component will be analyzed.

Nomenclature

ABS	acrylonitrile butadiene styrene
DSC	differential scanning calorimetry
EAM	extrusion-based additive manufacturing
AM	additive manufacturing
PIM	powder injection moulding
PLA	polylactic acid
SA	stearic acid
SEM	scanning electron microscope
EDX	energy dispersive X-ray

2. Material used

2.1. *Binder*

The binder is composed of a backbone polymer associated to a surfactant additive to ensure the wettability of the powder. Additionally, the surfactant lowers the shear viscosity. Melting temperatures are obtained by DSC analysis with 3 thermal cycles from 25 to 200°C at a rate of 5°C*min-1. The binder is composed of 90 %vol. of PLA and 10 %vol. of SA, whose characteristics are detailed in Table 1.

Table 1. Binder components and physical properties

Component	Role	Melting temp. (°C)	Density	Ref
PLA	Backbone	181 ± 2	1.25	[11]
SA	Surfactant	72 ± 2	0.94	[14]

2.2. *Powder*

The studied powder is a high carbon tool steel, whose designation is X 1,28 W Mo Cr V 6-5-4-3. The powder is obtained by gas atomization and sieved with a 45µm. Its commercial designation is PEARL® micro 2023. The shape of the powder, illustrated in Figure 1, has been obtained by SEM analysis, shows a spherical and smooth shape with very few satellites. This powder grade presents excellent mechanical properties and excellent corrosion resistance after all the heat treatments.

Fusion temperature is obtained with a dilatometry analysis performed in a SETSYS Evolution TMA with a thermal cycle from 25°C to 1300°C at 25°C*min^{-1} under an Argon atmosphere. The melting temperature of the powder is the limiting temperature during densification, as during the sintering process the powder grain fuse and diffuse in a solid state. Melting would cause a collapse of the geometry of the part resulting in the loss of the printed geometry.

Table 2. Powder characteristics.

Component	Role	Melting temp.(°C)	Density	d50 (µm)
Pearl® micro 2023	Powder	1280 ± 10	7.72	29

2.3. *Feedstock*

The critical and maximal powder volume loading values are optimized with the incremental mixing method like the one used by Royer et al.[7]. In a heated twin screw mixer, the powder is added progressively to the binder. It permits to evaluate the optimum powder charge in the feedstock [15].

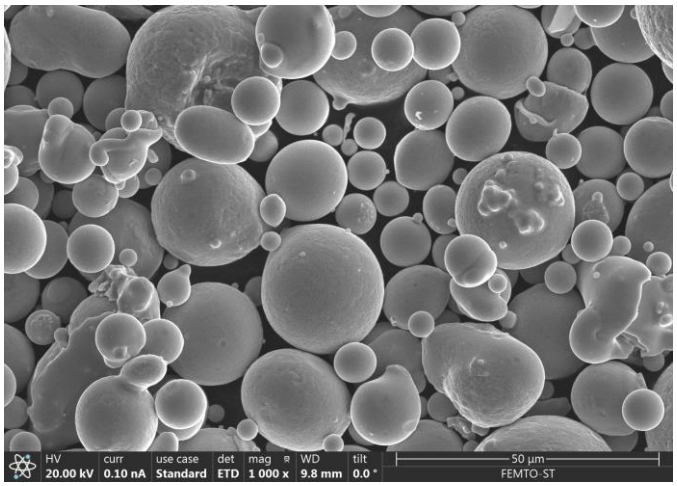

Figure 1. Pearl® Micro 2023 powder under SEM analysis

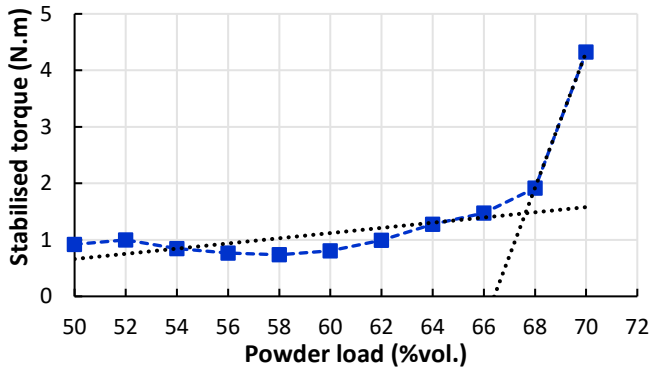

Figure 2. Incremental mixing of the binder and powder.

Increasing the powder volume rate causes an increase of the final stabilized torque and an increase of the final shear viscosity value of the developed feedstock dedicated to PIM-like EAM process [6].

Once the maximum powder loading rate is reached, the torque value will increase exponentially and will no longer provide a homogeneous mixture with the physical properties required for printing [7]. In a Plastograph EC W50EHT twin-screw mixer heated to 190°C and operating at 30 rpm, the incremental mixing of the binder and powder is shown in fig 2.

The incremental blend shows a sudden increase to 70%vol. The trend line of unsaturated and saturated mixtures crosses at 68%vol. which is the optimum powder load, Figure 2. At this highest powder volume rate value of the powder, the mixture remains homogeneous and printable. The feedstock used in this current work has a composition of 68%vol. of Pearl micro 2023 powder, 28.8%vol. of PLA and 3.2%vol. of SA.

A thermogravimetric analysis of the feedstock is performed to determine the best debinding kinetics (optimal temperature and debinding rate) to optimize debinding process. The thermogravimetric analysis is realized in a Netzsch STA 449C from 25 to 1000°C at 10°C*min^{-1}. Based on the result of figure 3, the TGA thermogram shows a peak in material weight loss

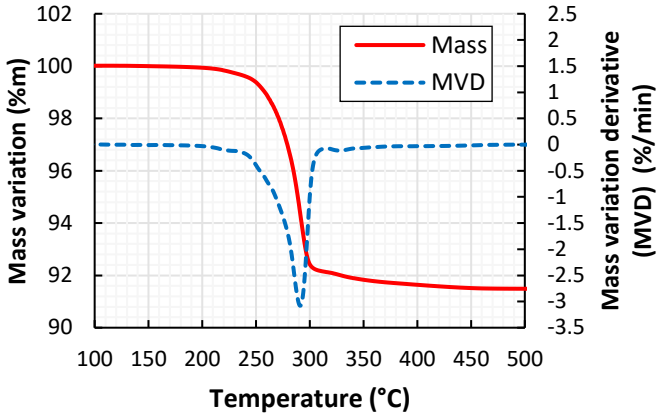

Figure 3. Thermogravimetric analysis of the feedstock between 100°C and 500°C

Figure 4. Front view of a cylinder part printed with the reference dimensions with a height of 10 mm and a diameter of 8 mm

speed at 291°C and an end of the peak at 305°C.

A temperature of 300°C is chosen for the debinding step because at this temperature the binder is almost completely degraded. The remaining binder serves to maintain the shape of the component and is removed during solid state sintering.

3. Part creation

3.1. *Fused deposit modeling 3D printing process*

Printed cylinder parts have a diameter of 8 mm on a height of 10 mm. They are created using an innovative, pellet-fed Distudio 3D extrusion head mounted on a 3D printer that allows for pellet-based printing instead of calibrated extruded filament. 3D printing nozzle has a cylindrical outlet diameter of 0.8mm. The nozzle is heated to 200°C and the printing bed, to 60°C. The geometry is up in layers of 0.3 mm. The parts are printed with 100% filling, and the density obtained is 97.7±1%, see figure 4. The crystallization of the layers is not controlled

as the mechanical characteristics of the created part are not used in this study, so delamination is not an issue [16].

The surface quality is fairly bad, even for raw additive manufacturing processes.

3.2. *Debinding*

The printed parts are debinded by thermal degradation of the PLA and SA polymers. The thermal cycle is carried out in a neutral nitrogen atmosphere to avoid oxidation. It starts at 25°C to reach 300°C at 30°C*h^{-1} and is maintained at 300°C for 1h. The duration of the thermal debinding stage is much faster than the one when using polyethylene or polypropylene binders [7]. The debinded printed part are obtained without external defects and are used for the following sintering stage.

An additional TGA analysis performed on debinded sample measures that the remaining binder is equivalent to 0.03%wt validating the debinding cycle.

3.3. *Sintering*

Densification by natural sintering is performed in a SETSYS Evolution TMA. The critical temperature for the sintering process is below 1280°C, and further tests show that a sintering temperature of 1250 °C gives the best results. The time-at-temperature has a tangible influence on the surface quality, as the restructuring of grains by capillary forces creates a smoother surface. The sintering cycle consists of two parts: first the debinding is carried out under vacuum, with a temperature rise to 500°C for 10min, then the sintering takes place at 1250°C under a neutral argon gas atmosphere, with a variable temperature time. The thermal kinetics is 50°C*min^{-1}.

4. Results

4.1. *Surface rugosity*

Figure 5, shows a zoom of the surface of the sintered parts at 1250°C with different holding times ranging from 0.5h, to 2h and finally 3.5h for a), b) and c), respectively. An increase of time-at-temperature has a direct impact on the smoothness

of the sintered surface. The sintered print layers are not visible in the cylinder component when the temperature time is greater than 3.5 h.

The surface roughness measured with an ALTIMET Altisurf 520 longitudinally every 90° for each part is presented in Figure 6. The measured profiles are discretized and filtered with a Gaussian filter and a cut-off of 2.5 mm. It shows that the surface roughness is reduced by a factor of 3 when sintering for a time-at-temperature of 0.5 h or 2 h and by a factor of 5 when sintered with a time-at-temperature of 3.5 h or 5 h.

Figure 7 (a), (b) and (c) shows a profile measured from the printed green component to the final sintered component for two time-at-temperatures at 0.5 h and 2 h. The value of the

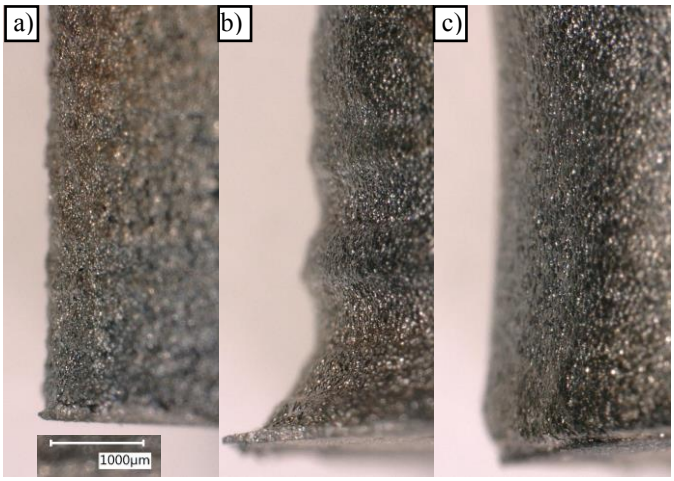

Figure 5. Surface Picture of the sintered parts for a time-at-temperature of: a) 0.5 h, b) 2 h, c) 3.5 h under an optical microscope with a x50 zoom.

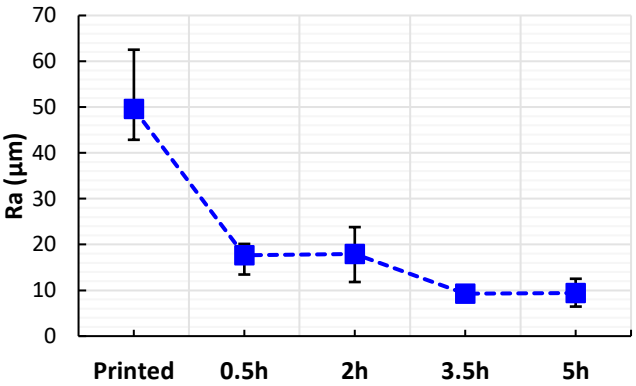

Figure 6. Measured arithmetic rugosity (Ra) versus Time-at-temperature

surface profile obtained from the printed part to the densified component decreases after the sintering and densification steps. In addition, the best value is obtained for the longest sintering time of 5 h.

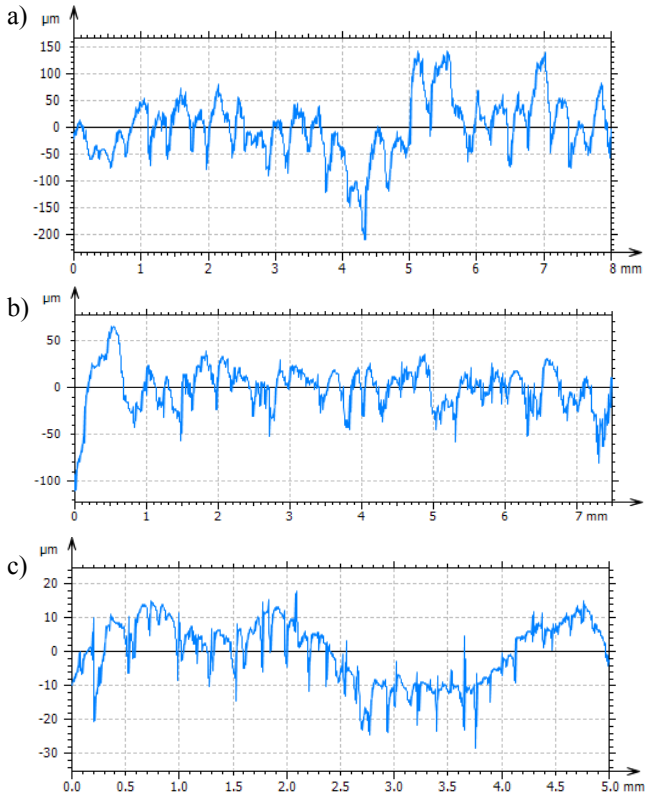

Figure 7. Surface profile for a) a printed sample, sintered sample with a time-at-temperature of b) 0.5h and c) 5h.

4.2. Surface quality

The porosity of the sintered parts is measured at 2.64%, 2.76% and 2.78% for a time-at-temperature of 0.5h, 2h and 3.5h respectively. This value already validates all the debinding and densification stages that have been developed and also indicates a low porosity value allowing the final heat treatment by Hot Isostatic Pressing (HIP) process to obtain a fully dense final component with excellent functional properties.

Sintered parts are sliced and polished to observe their microstructure (figures 8 and 9). While a time-at-temperature of 0.5 h (figure 8) shows a difference between the surface and the center of the part, with a surface structure of 0.2 mm depth, a time-at-temperature of 2 h (figure 9) shows that this surface layer is 0.4 mm. An increase in time-at-temperature is correlated with an increase in the thickness of this outer layer.

In addition, the microstructure is more advanced in Figure 9, as the grains at the center are smaller with more defined and rounded edges. The heavier elements of the steel alloy are grouped in the whiter grains (molybdenum and tungsten) and create dendritic structure, which separate the darker, more ferrous central grains. Other grey grains, visible only in Figure 9, contain a majority of the other elements (chromium, carbon, vanadium) and a minority of molybdenum.

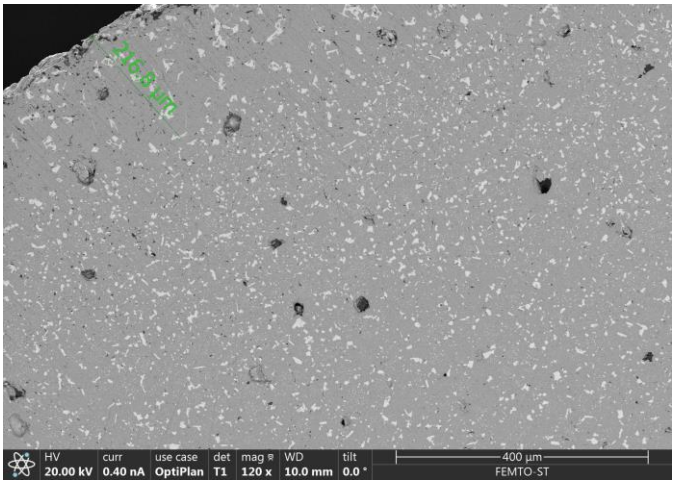

Figure 8. SEM observation of a cross-section of a sample with a time-at-temperature of 0.5h. EDX analysis.

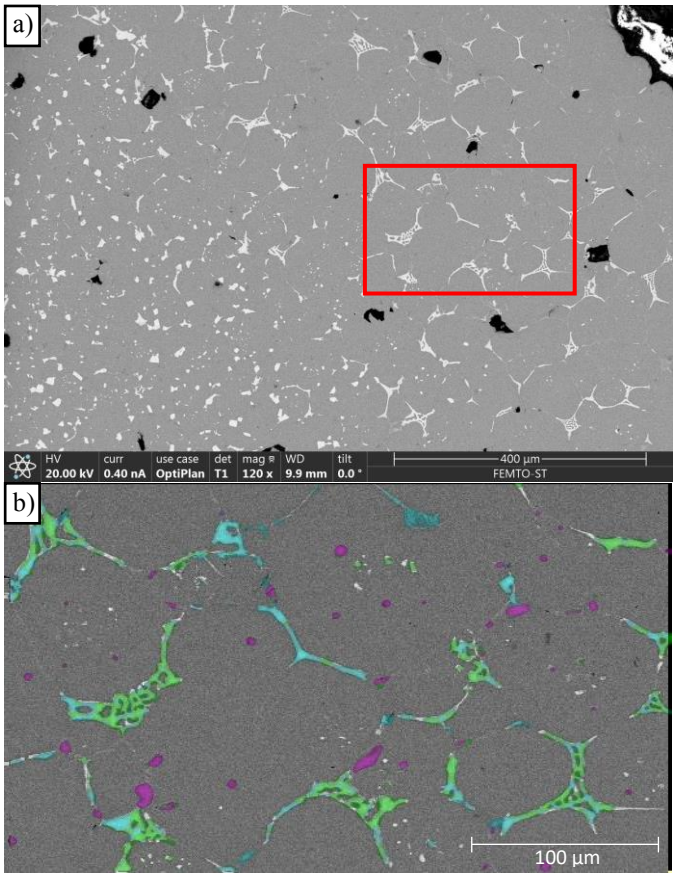

Figure 9. SEM observation of a cross-section of a sample with a time-at-temperature of 2h. a) EDX analysis and b) colorized EDX analysis with Tungsten in green, Molybdenum in cyan and Vanadium in pink. Other elements are not colorized.

5. Conclusion

This work on PIM-like EAM shows that the process can be applied using a bio-polymer binder and that the use of a high alloy steel powder is not a problem in this process; with the

developments made components having been obtained at each stage of the process without external defects. The thermal debinding and densification kinetics times that have been used are short and lead to a low porosity value.

Time-at-temperature during sintering is critical to optimize the micro-structure and surface roughness.

An increase of time-at-temperature leads to a smoother surface that overturn the initial high rugosity and a larger surface layer.

Acknowledgments

The research was supported by the EIPHI Graduate School (contract ANR-17-EURE-0002) including its experimental facilities (manufacture of the high loaded feedstock, printing and optical 3D metrology). The authors are grateful to MIFHySTO technological platform for the use of equipment. Some of the work in this article was created with the Renatech platform.

References

[1] Rane, K., Strano, M. ,2019. A comprehensive review of extrusion-based additive manufacturing processes for rapid production of metallic and ceramic parts. *Advances in Manufacturing*, vol. 7, no 2, p. 155-173.

[2] Peng, E., Zhang, D., Ding, J., 2018. Ceramic robocasting: recent achievements, potential, and future developments. *Advanced Materials*, vol. 30, no 47, p. 1802404.

[3] Valino, A. D., Dizon, JR.., Espera, A., et al., 2019. Advances in 3D printing of thermoplastic polymer composites and nanocomposites. *Progress in Polymer Science*, vol. 98, p. 101162..

[4] Maguire, A., Pottackal, N., Saadi, M. A. S. R., et al. 2021. Additive manufacturing of polymer-based structures by extrusion technologies. *Oxford Open Materials Science*, vol. 1, no 1, p. itaa004.

[5] Park, S., et al., 1990. Rapid manufacturing of micro-drilling devices using FFF-type 3D printing technology. *Scientific Reports* 11.1 (2021): 1-9.

[6] German, R. M., et al., 1990. *Powder injection molding*.

[7] Royer, A., Barrière, T., GELIN, JC., 2016. Development and characterization of a metal injection molding bio sourced inconel 718 feedstock based on polyhydroxyalkanoates. *Metals*, vol. 6, no 4, p. 89.

[8] Dong, J., Tümer, N., Putra, N. E., et al., 2021. Extrusion-based 3D printed magnesium scaffolds with multifunctional MgF 2 and MgF 2–CaP coatings. *Biomaterials Science*, vol. 9, no 21, p. 7159-7182.

[9] Jiang, D., Ning, F., 2022. Anisotropic deformation of 316L stainless steel overhang structures built by material extrusion based additive manufacturing. *Additive Manufacturing*, vol. 50, p. 102545.

[10] Singh, G., Missiaen, JM., Bouvard, D., et al., 2021. Additive manufacturing of 17–4 PH steel using metal injection molding feedstock: Analysis of 3D extrusion printing, debinding and sintering. *Additive Manufacturing*, vol. 47, p. 102287.

[11] Eynde, MVD. et Puyvelde, PV., 2017. 3D Printing of Poly (lactic acid). *Industrial Applications of Poly (lactic acid)*, p. 139-158.

[12] Fan, Y., Nishida, H., Shirai, Y., et al., 2004. Thermal degradation behaviour of poly (lactic acid) stereocomplex. *Polymer Degradation and Stability*, vol. 86, no 2, p. 197-208.

[13] Myers, N. S., Heaney, D. F., 2012. Metal injection molding (MIM) of high-speed tool steels. *Handbook of Metal Injection Molding. Woodhead Publishing,* p. 516-525.

[14] Momeni, V., Askari, A., Allaei, M. H., et al., 2021. Investigating the effect of Stearic Acid on the mechanical, rheological, and microstructural properties of AISI 4605 feedstock for metal injection molding process. *Transactions of the Indian Institute of Metals*, vol. 74, no 9, p. 2161-2170.

[15] Kong, X., Barriere, T., Gelin, J. C., 2012. Determination of critical and optimal powder loadings for 316L fine stainless steel feedstocks for micro-powder injection molding. *Journal of Materials Processing Technology*, vol. 212, no 11, p. 2173-2182.

[16] Abid, M., Mallet, B., Lamnawar, K., et al., 2018. Crystallization of Poly (Lactic Acid), PLA: Effect of Nucleating Agents and Structure-Properties Relationships. *Journal of Composites and Biodegradable Polymers*, vol. 6, p. 34-46.